TWO-DIMENSIONAL INFRARED DETECTOR ARRAYS

C. R. McCreight
NASA Ames Research Center
Moffett Field, CA 94035 USA

Abstract

The technology and terminology of integrated infrared detector arrays are discussed. Specific infrared array multiplexer designs include the charge-coupled device (CCD) and charge-injection device (CID). Laboratory data and telescope imagery obtained with three arrays (InSb CCD, Si:In CCD, and Si:Bi CID) are used to illustrate the performance and promise of integrated arrays in astronomical applications.

Introduction

Recent advances in microelectronics technology have made possible the production of multiple-element arrays of infrared (IR) detectors. These devices incorporate various schemes for multiplexing signals from the individual array elements. A number of promising astronomical applications for IR arrays can be envisioned, including direct imaging, spectroscopy, polarimetry, and speckle observations.

In this paper, an introduction to overall IR array concepts and particular array designs, and examples of laboratory and observational data obtained with IR arrays will be presented. It is important to keep in mind that this is a rapidly-developing area, where experience is still rather limited and devices are in a state of active development. The promise of IR arrays for astronomical applications is very real, but it is based on the experience of a small number of investigators, since devices are still not widely available to the astronomical community. Much remains to be done, in terms of improving both the basic device characteristics and the knowledge of ways to effectively utilize arrays in astronomical instrumentation.

IR Array Concepts and Terminology

Integrated IR arrays differ in a number of respects from the discrete IR detector technology from which they evolved. Because of their larger size, multiple-element integrated arrays generally require larger single crystals of detector-grade semiconductor material. In practice this, and the need to

Proceedings of the IAU Colloquium No. 79: "Very Large Telescopes, their Instrumentation and Programs", Garching, April 9–12, 1984.

maintain excellent process control over relatively large areas, mean that the overall production yield of arrays can be quite low. On-chip integration of signals is a fundamental operating principle of integrated IR detector arrays, which contrasts with the continuous readout of conventional discrete detectors; on-chip integration offers a potential sensitivity advantage. Since photolithographic masks are used in their production, this allows integrated arrays to achieve a built-in, precise registration of relatively large numbers of array elements (pixels). Fig. 1 shows a representation of a fully-multiplexed integrated array, with a single output preamplifier for all array elements. This feature allows dramatic simplifications within instrument systems (e.g. reducing the number of electrical connections to the focal plane, and the amount of on-chip power dissipation) as compared to an array of discrete detectors. Integrated arrays have the capability of producing substantial amounts of information, which presents the need for a computer-based data system to keep up with the array data rate, and a well-conceived software system for managing and displaying the data. Particularly for imaging applications, procedures such as flat-fielding, which involve additional observational and data-processing procedures, are required when utilizing arrays.

Multiplexing is the approach which allows the practical implementation of large arrays. Either in a totally-multiplexed serial fashion, or in various parallel-serial architectures, signals detected at each element are sequentially routed to warm processing electronics. One requires both clocked voltage waveforms and various DC levels to operate an IR array multiplexer; for good system sensitivity, these voltages must be free from noise and oscillations, and capacitive coupling must be minimal.

In discussing IR arrays, one confronts a new terminology along with the new principles of operation. Fig. 2 illustrates the features of a charge-coupled device (CCD) array[1], and provides a useful example of the functions and terms associated with an integrated array. The charges generated in the array (charge packets) are collected in potential wells or "buckets". In the CCD, these wells are created at the interface between the detector material and an insulating oxide layer. Application of the proper voltages on the metal gates deposited over the oxide creates a local depletion region where optically-generated (and other) charges can collect. The charge packets are transferred laterally in the multiplexer by the creation of a potential well adjacent to the initial location. Shortly thereafter, the initial well is collapsed and the charge is moved one increment closer to the output stage, which completes the elemental transfer. This process continues until all charge packets are serially shifted

to and sensed at the output preamplifier. In an IR CCD array, every third (or fourth) gate is tied to a common clock voltage; this defines a three (or four) phase multiplexer. The multiplexer shown in Fig. 2 is obviously three-phase. The effectiveness of the CCD charge transfer process is characterized by the charge transfer efficiency, which is that fraction of a charge packet which survives in a single transfer. Charge transfer efficiencies of 0.999 to 0.9999 have been demonstrated in good IR CCD arrays.

Due to their low operating temperature, IR CCD arrays must use surface-channel CCD multiplexers, wherein the charge packets are shifted along the interface between the substrate and the oxide. A less-noisy alternative, which is commonly used in optical CCDs, is the buried-channel structure[2], which involves storage and shifting of the charge along a p-n junction implanted some fraction of a μm below the surface, away from surface state traps and their associated noise. Due to carrier freeze-out, buried channel silicon CCD structures are not useful at low temperatures.

The process of sensing the charge packets at the multiplexer output node involves noise from various sources; the noise of the preamplifier itself often dominates. Due to the charge-integration process and the discrete-sampled nature of the output stream, a characteristic of the array is its read noise, which represents a fixed noise penalty encountered every time the array is read out, irregardless of whether the well is empty or full. The read noise adds in quadrature with other array noise sources, such as photon noise.

Referring again to Fig. 2, a limit is encountered in the amount of charge which can be stored under a gate of given dimensions and an insulating layer of given dielectric properties and thickness. This limit is known as the well capacity, which in a good IR array is on the order of 10^7 electrons. The dynamic range of the device is simply the ratio of the well capacity to the read noise (for unit signal/noise). Finally, one encounters crosstalk in an IR array, which is a signal in a given pixel which has been coupled in from an adjacent pixel by electrical or optical means. A crosstalk level of 5% or less can be expected in most IR arrays.

Array Design Approaches

A basic feature of an IR array is the function and geometry of its integral multiplexer. Infrared integrated arrays were initially produced in monolithic form[3], in analogy to optical arrays, where the charge detection and charge

https://doi.org/10.1017/S0252921100108693 Published online by Cambridge University Press

transfer processes were accomplished in a common substrate. A monolithic structure is shown schematically in Fig. 3. This approach has largely been superceded by hybrid designs[4], where separately produced and optimized detector and multiplexer substrates are precisely aligned and then interconnected with small metal bumps. (A hybrid array is illustrated in Fig. 1.) This bump-bonding or "flip-chip" process has proven to be reliable, and 100% interconnect yields are not uncommon. The hybrid approach allows a wide variety of detector materials to be used with a general-purpose silicon multiplexer, and besides CCDs, one can bump-bond other types of multiplexers [e.g. switched field effect transistor (FET) multiplexers] to detector substrates.

IR CCD arrays generally have good charge-storage capacity and frequency response. They also provide fully-multiplexed output. With intrinsic materials one can achieve quantum efficiencies on the order of 50 - 60%, while with extrinsic materials, these values are in the 30% range. Generally, IR CCD read noise levels are on the order of 1000 rms e^-, which limits their capability in very low background applications.

Another integrated array approach is the extrinsic silicon accumulation-mode charge injection device (AMCID).[5] (This device should not be confused with the dual-gate InSb CID.[6]) As shown in Fig. 4, charge in an AMCID is generated in the substrate and then attracted to and stored beneath a local gate, which is deposited on an oxide layer. During the integration period, a positive potential is applied to the gate. During the brief readout cycle, the polarity of this voltage is reversed, which drives the charge packet through the substrate to the input capacitance of a cold FET. A load resistor is included for passive reset of this node, so the charge packet must be sampled immediately after the readout pulse is removed. An array of these gates is produced on a common substrate, and digital CMOS circuitry on the focal plane provides the sequential readout pulses to the various columns of pixels. A 16 x 16-element AMCID array is illustrated in Fig. 5. This type of device has the advantage of structural simplicity and good read noise levels, on the order of 100 - 200 rms e^-. Responsive quantum efficiencies in the 25 - 30% range have been reported.[5] The AMCID can, however, have limited well capacity and frequency response, particularly under reduced-background conditions, and the difficulties in depositing thin high-quality oxide layers on detector-grade material have resulted in low AMCID production yields.

A more recent development involves the switched-FET or switched-sample photoconductor technique. A conventional photoconductor, without an oxide

layer, is used as the detector element, and charge is integrated on the gate of a dedicated FET. MOSFETs act in this circuit as capacitors whether or not they are conducting, so an array of elements, each with dedicated FETs (as a minimum, one for charge storage, and another for active reset after readout), can integrate signal and be read out in sequence. (Note that, as with the AMCID configuration, one output line per row of the array is required, i.e. a switched-FET array with 16 columns and 8 rows would have 8 signal lines out of the dewar.) The unit cell of a two-dimensional array is shown in Fig. 6. The prime advantages of this approach are producibility and low noise. With a switched-FET array, one would expect responsivities and read noise levels comparable to those achieved in an AMCID, without the low yield and irregular effects they exhibit.

As was mentioned above, an essential element in a useful IR array-based instrument is an effective data system. An example of a useful system, developed at Ames[7], is shown in Fig. 7. Commercial components and architectures were used throughout this Z80-based microcomputer system. The only unique element of the system is the TTL co-processor stage, which performs real-time additions or subtractions of the frame data on a pixel-by-pixel basis, depending on the position of the chopping secondary mirror (which is driven by the computer). At the end of an integration period, typically on the order of minutes, the accumulated frame data are downloaded to the computer for quick-look processing and display. A previous version of the system involved transmission of analog signals from the telescope to the control room; the latest configuration (Fig. 7) is significantly improved, with simplified cabling, transmission of digital data, and better immunity from noise and pickup.

Astronomical Applications of IR Arrays

To illustrate astronomical results obtained with integrated IR arrays, three examples of recent observing projects will be discussed. Note that the arrays used were obtained from three different sources. Table I is a compilation of information about each device and project.

The hybrid 32 x 32 InSb CCD array[8], supplied to W. Forrest and J. Pipher of the University of Rochester by Santa Barbara Research Center, has been thoroughly characterized in the laboratory, and successfully used in observational programs. Parametric studies of operating temperature, the various dc and clocked voltages, and readout frequencies were completed in the

https://doi.org/10.1017/S0252921100108693 Published online by Cambridge University Press

laboratory. Astronomical results obtained in spring of 1983 include imagery of the M82 galaxy (Fig. 8), Saturn (Fig. 9), and the Orion nebula (Fig. 10) at various wavelengths. Subsequent observations at Kitt Peak National Observatory with an improved dewar also produced excellent imagery. During this latter run, it was possible to integrate signal on the chip for up to 4 min. Results from this series were used to estimate the sensitivity of the system in an actual observing situation; a limiting magnitude of 17.5 at 2.2 μm (i.e. 64 μJy for a 355 s integration time, 1σ noise, 0.41 μm bandwidth) was obtained, which compares quite favorably with the sensitivity of discrete-detector systems.

In a collaboration between Rockwell International and the University of Hawaii (R. Capps), laboratory and telescope data have been obtained with a hybrid 32 x 32 Si:In CCD array.[9] A flat-field image from that array is shown in Fig. 11. This array included a region near its center where pixels were not successfully mated to the multiplexer. Fig. 12 is a composite view of imagery obtained with this array at the Infrared Telescope Facitity (IRTF). In the lower left, the 3.5 μm image of a point source (α Ori) is shown; the remainder of the figure clearly shows the spatial extent of the bipolar nebula OH 0739-14. The latter image is a composite of nine individual frames which have been flat-fielded, i.e. the pixel-to-pixel gain variations have been corrected out. Note, however, that the effect of the dead spot in the center of the array has not been removed. In addition, limited telescope testing with short (50 ms) integration times has proven successful in displaying speckle patterns. An individual 3.5 μm speckle pattern from α Ori is displayed in Fig. 13.

The final examples were obtained with two nearly identical 16 x 16 Si:Bi AMCID arrays from Aerojet ElectroSystems Company. In tests with a circular variable filter wheel dewar, J. Goebel and his colleagues obtained 3 μm imagery of various point sources and planets with AMCID "array #1." Fig. 14, an image of α Ori, illustrates the horizontal (i.e. row-to-row) crosstalk, on the order of 25%, which is characteristic of two-dimensional AMCID arrays. This crosstalk is caused by capacitive coupling between the closely-mounted output FETs in the array. The vertical (i.e. column-to-column) crosstalk was found to be about 5%.

Another 16 x 16 Si:Bi AMCID array (#2) was used by D. Gezari, G. Fazio, W. Hoffmann et al. for lab tests and observations in the NASA Goddard 10 μm Camera System.[10,11] In August 1983, impressive imagery was obtained at the IRTF. Fig. 15 shows a high-spatial-resolution map of the galactic center at 8.3 μm which was assembled from approximately 10 individual frames. The planetary nebula NGC 7027 was also well-resolved in each of four color bands (Fig. 16). For both of

these results, array frame rates of about 700 Hz were used, with a chopping frequency of 10 Hz; typically 1 min of total integration time was used in each observation. The total sensitivity of the camera system was estimated to be 2 Jy for 1 min of integration, and a nominal 5% filter bandwidth.

Discussion

For most ground-based applications with moderate to low spectral resolution, one would expect IR detector arrays to be background-noise-limited. When system performance is limited by the background, one desires a maximum quantum efficiency and well capacity. In the spectral range shortward of about 12 μm, various intrinsic photovoltaic (e.g. InSb) and extrinsic photoconductive (e.g. Si:In) IR arrays are available; the particular choice of an optimal array must rely on the detailed characteristics of various candidate devices. For comparable levels of technological maturity, one would expect to achieve better sensitivity with an intrinsic array, with its superior quantum efficiency and the absence of recombination noise. For wavelengths beyond about 12 μm, various extrinsic silicon integrated arrays can be considered.

Integrated IR arrays, with their ability to generate impressive amounts of data, require rather sophisticated data collection and processing systems. One must design a data system which extracts and stores only essential information from the total data base, and which can display "quick look" information to guide the course of an observation. While these data systems are straightforward in concept, their detailed implementation can be quite challenging and time consuming.

In general, astronomical applications of integrated IR detector arrays are still in their initial phase of demonstration; it has been established that relatively bright objects can be successfully imaged. Preliminary but encouraging indications of array sensitivity have been obtained. The next steps in array development will involve more detailed laboratory characterizations, optimizations of devices specifically for astronomical applications, and observations of fainter objects. It is expected that more effective applications of array instruments will occur, with better instruments, support electronics, data systems, and observing strategies.

Although experience is limited and much remains to be done, there appears to be a good basis for optimism for integrated array technology in astronomical applications. It is highly significant that array sensitivities comparable to

https://doi.org/10.1017/S0252921100108693 Published online by Cambridge University Press

discrete-detector systems have been demonstrated in telescope applications, and that excellent spatial resolution and registration have been obtained in the images taken to date.

Acknowledgement

The continued support of NASA's Office of Aeronautics and Space Technology is gratefully acknowledged.

References

1. C. H. Séquin and M. F. Tompsett, Charge Transfer Devices, Academic Press, New York (1975).

2. A. F. Milton, in Optical and Infrared Detectors (R. J. Keyes, ed.), Ch. 6, Springer, New York (1977).

3. R. D. Thom et al., IEEE Trans. Electron Devices ED-27, 160 (1980).

4. J. T. Longo et al., IEEE Trans. Electron Devices ED-25, 213 (1978).

5. C. R. McCreight and J. H. Goebel, Appl. Opt. 20, 3189 (1981).

6. J. C. Kim, IEEE Trans. Electron Devices ED-25, 232 (1978).

7. P. S. Stafford and D. A Jared, Paper 83-2377CP, AIAA Computers in Aerospace Conference, Hartford, CT. October 1983.

8. W. J. Parrish et al., Technical Digest of International Electron Devices Meeting, Washington, DC. 513 (1978).

9. D. H. Pommerrenig et al., Proc. SPIE 267, 23 (1981).

10. J. F. Arens et al., Opt. Eng. 22, 267 (1983).

11. G. M. Lamb et al., Proc. SPIE 445, 113 (1983).

12. D. F. Barbe, Proc. IEEE 63, 38 (1975).

Table I. Comparison of IR Arrays Used in Observing Programs

	InSb CCD	Si:In CCD	Si:Bi AMCID
Format	32 x 32	32 x 32	16 x 16
Supplier	Santa Barbara Research Center	Rockwell International	Aerojet ElectroSystems Company
Lab Test at	U. Rochester	U. Hawaii	#1 NASA Ames #2 NASA Goddard
Approximate Useful Wavelength Range (μm)	1 - 5	2 - 8	3 - 17
Typical Operating Temperature (K)	40 - 60	35	10
Pixel Size (μm)	94	88	140
Telescope Test at	0.6m Mees, 1.3m KPNO	3m IRTF	#1 1.5m Mt. Lemmon #2 1.5m Mt. Lemmon, 3m IRTF
Angular Size of Pixel on Telescope (arcsec)	2.5 (Mees), 1.0 (KPNO)	0.2	#1 1.8 #2 1.3 (Mt. Lemmon), 0.8 (IRTF)

https://doi.org/10.1017/S0252921100108693 Published online by Cambridge University Press

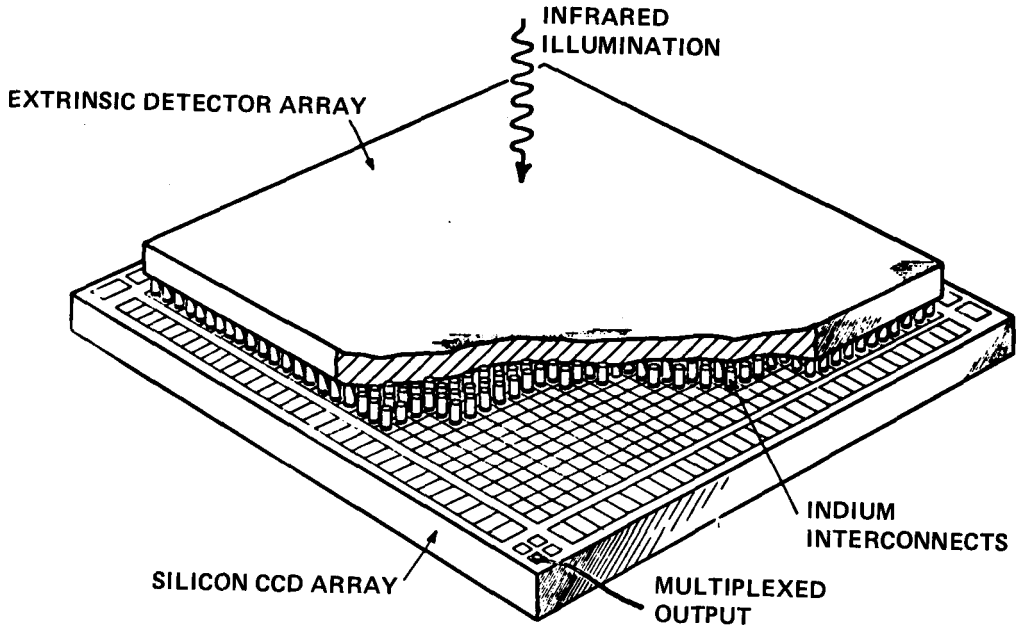

Fig. 1. Schematic view of a hybrid integrated infrared array.

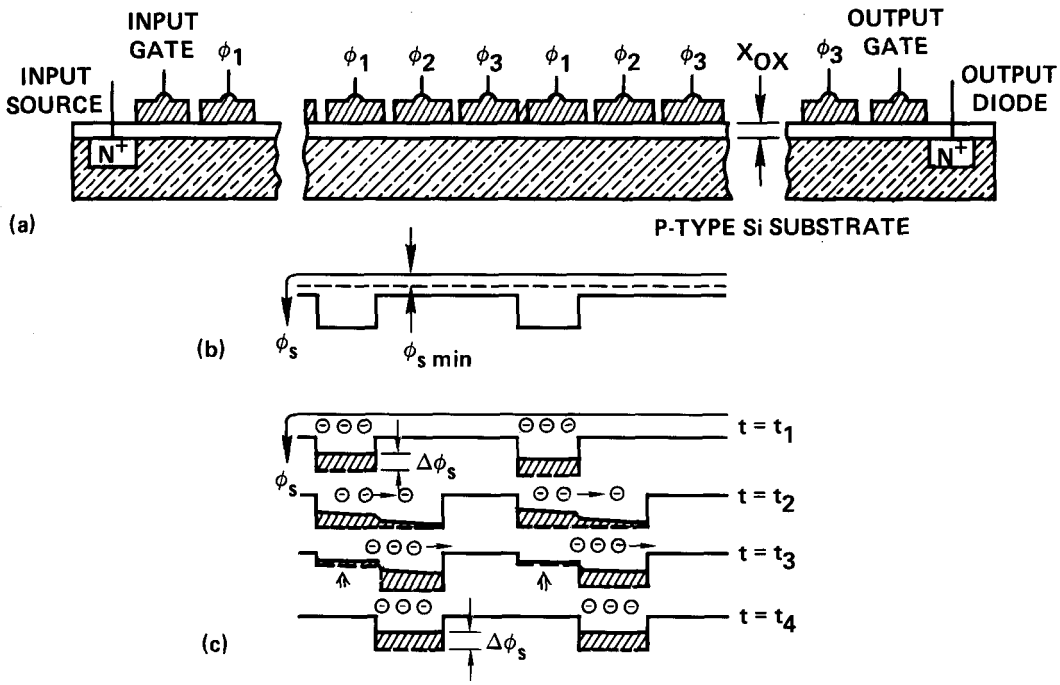

Fig. 2. Schematic of (a) three-phase CCD array, (b) potential well, and (c) elemental transfer of a charge packet (Ref. 12).

https://doi.org/10.1017/S0252921100108693 Published online by Cambridge University Press

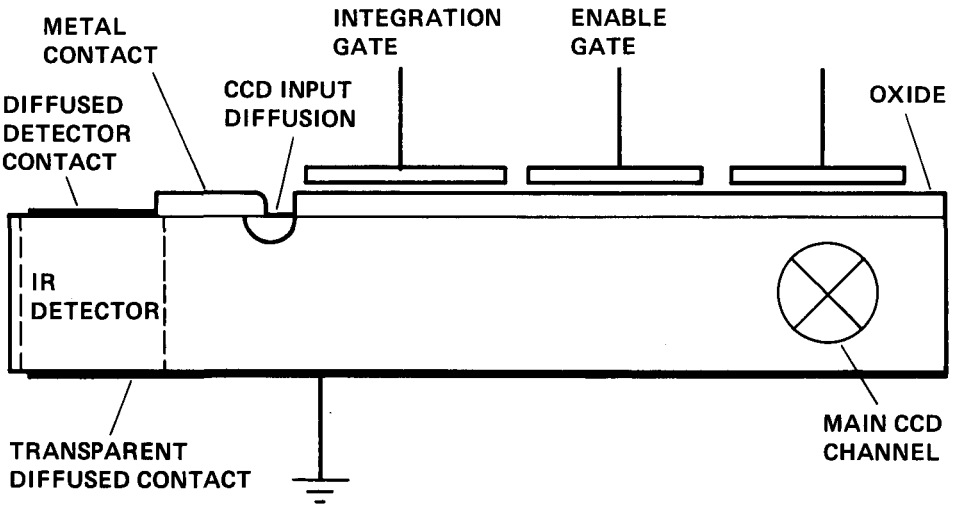

Fig. 3. Monolithic integrated infrared charge-coupled device array.

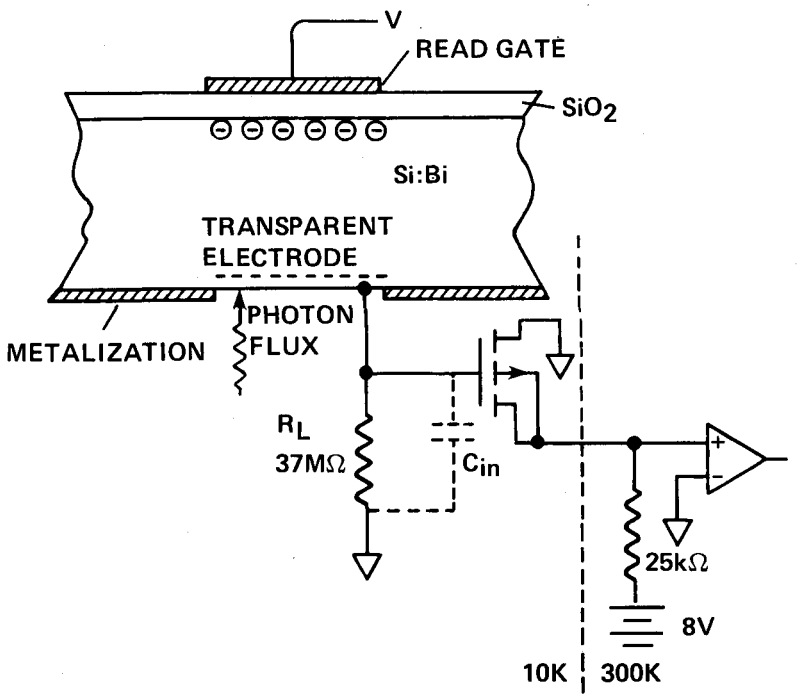

Fig. 4. Unit cell of an accumulation-mode charge injection device.

https://doi.org/10.1017/S0252921100108693 Published online by Cambridge University Press

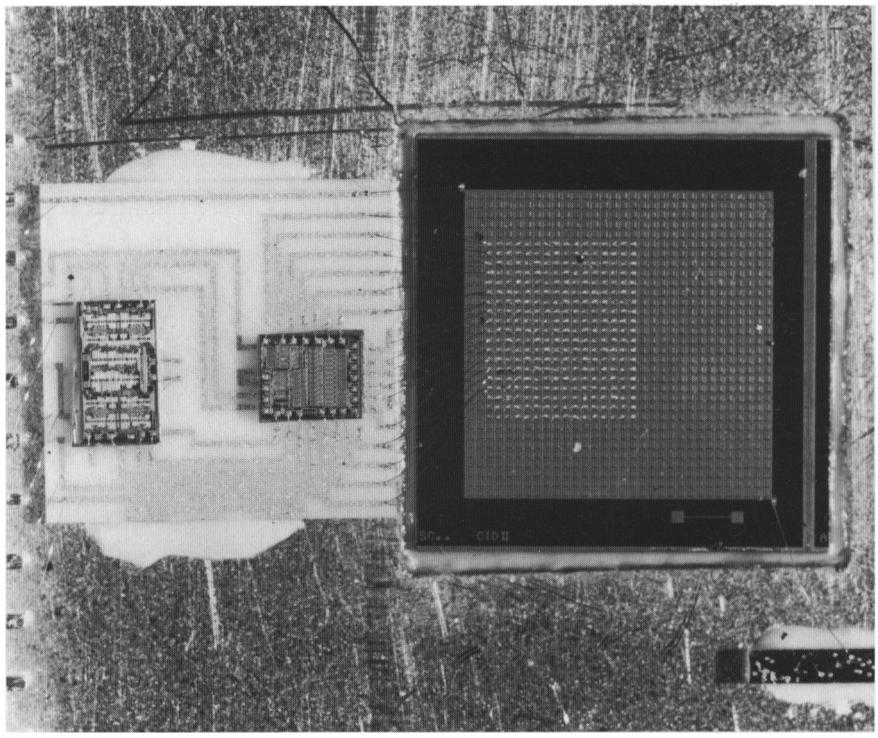

Fig. 5. Photograph of 16 x 16 Si:Bi AMCID array. To the left are CMOS scanning electronics. The detector substrate, about 6.5 mm on a side, appears on the right.

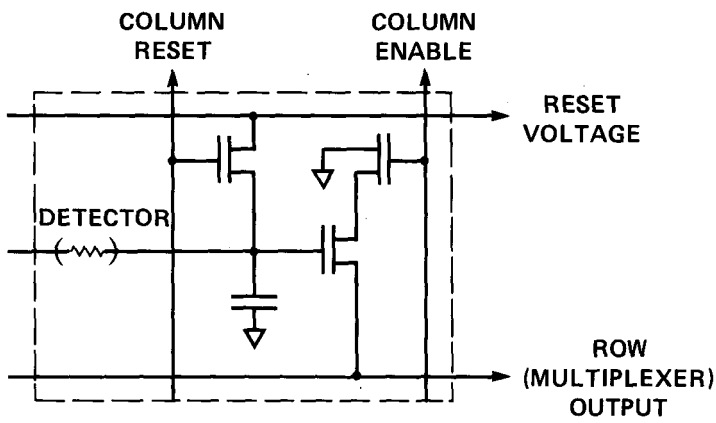

Fig. 6. Unit cell of a switched-FET IR array.

https://doi.org/10.1017/S0252921100108693 Published online by Cambridge University Press

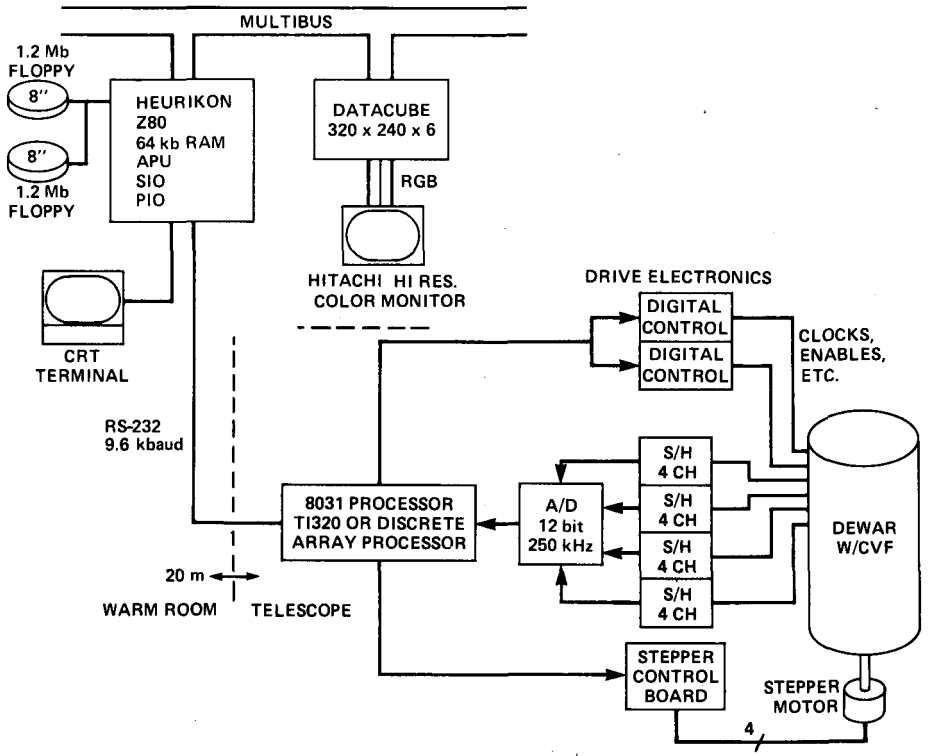

Fig. 7. IR array data collection and processing system.

Fig. 8. 2.2 μm image of M82 galaxy obtained with InSb CCD array at Mees Observatory. North is at the top; east is to the left. Total field of view is 80 arcsec. Moving clockwise from the upper left, the video display was scaled to 1x saturation; 2x saturation; 8x saturation; and 4x saturation.

https://doi.org/10.1017/S0252921100108693 Published online by Cambridge University Press

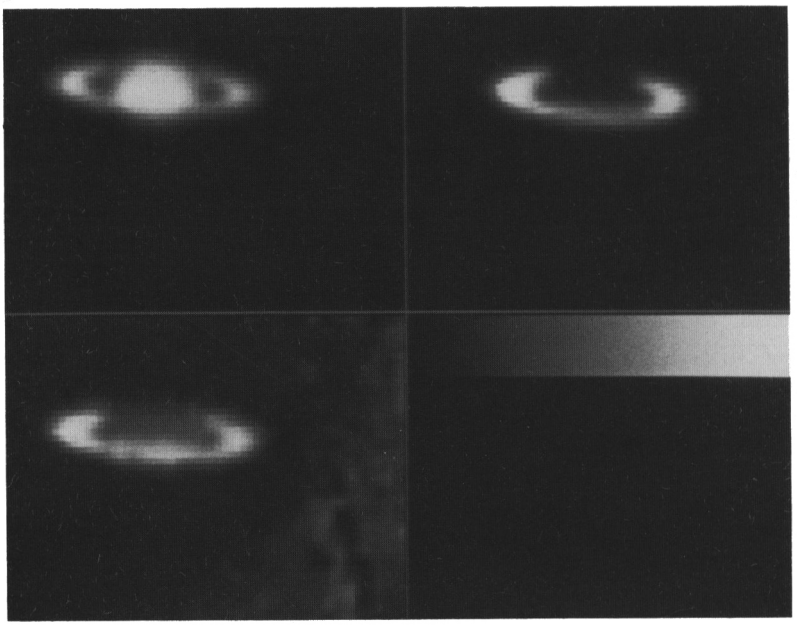

Fig. 9. Images of Saturn taken with InSb CCD array, Mees Observatory. Upper left is 1.65 μm; upper right is 2.2 μm; lower left is 3.75 μm.

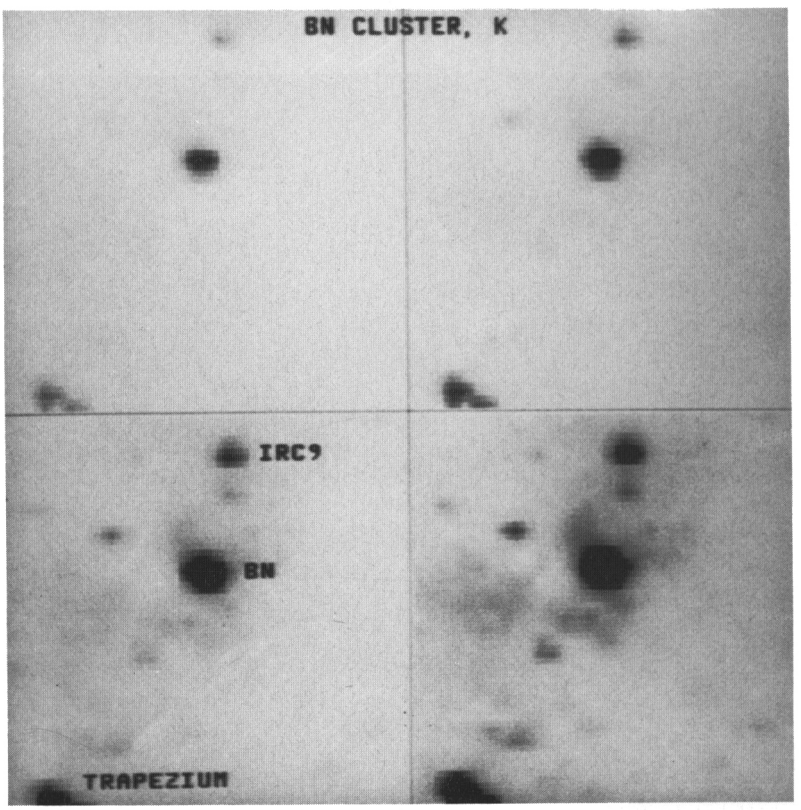

Fig. 10. 2.2 μm InSb imagery of Orion nebula taken at Mees Observatory. Total field of view = 80 arcsec. Moving clockwise from the upper left, display was scaled to 1x saturation; 2x saturation; 8x saturation; and 4x saturation.

https://doi.org/10.1017/S0252921100108693 Published online by Cambridge University Press

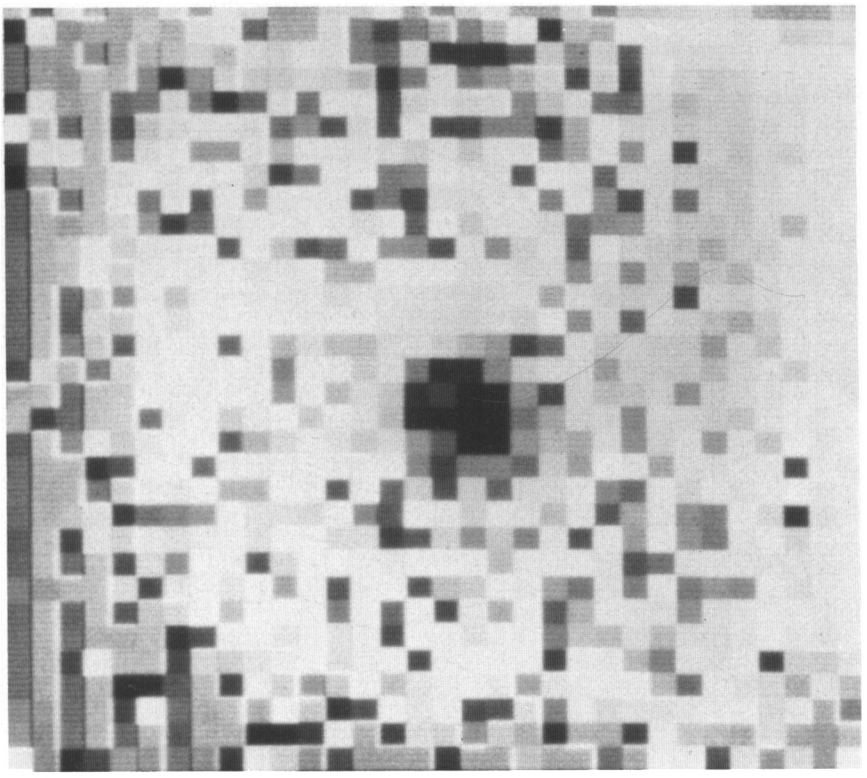

Fig. 11. Flat-field image obtained with 32 x 32 Si:In CCD array.

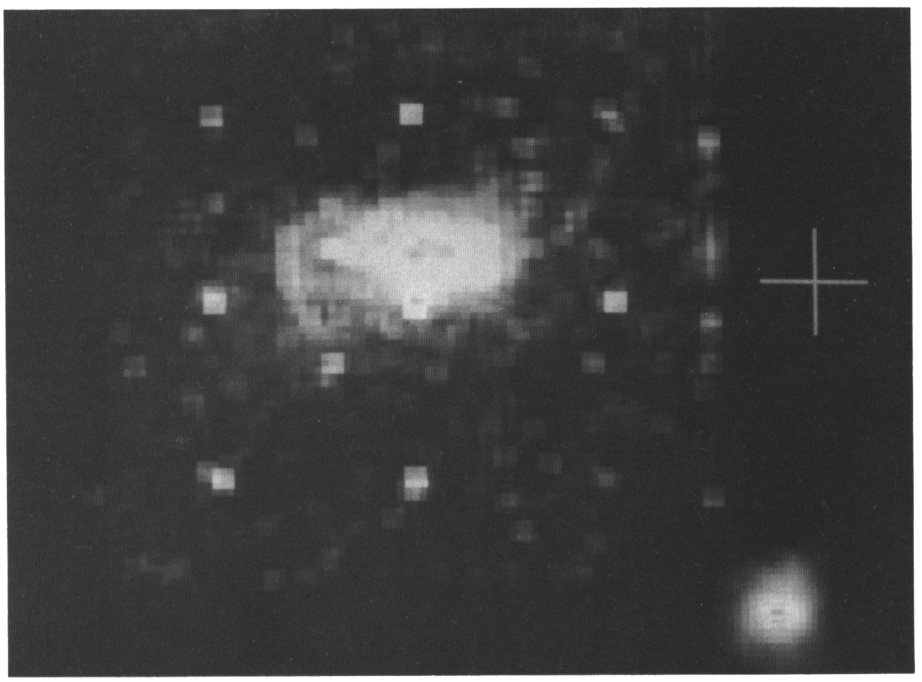

Fig. 12. Composite of two 3.5 μm Si:In CCD array images taken at IRTF. Image at lower right is α Ori. Remainder of figure is an image of OH 0739-14, with a total field of view of about 18 arcsec.

https://doi.org/10.1017/S0252921100108693 Published online by Cambridge University Press

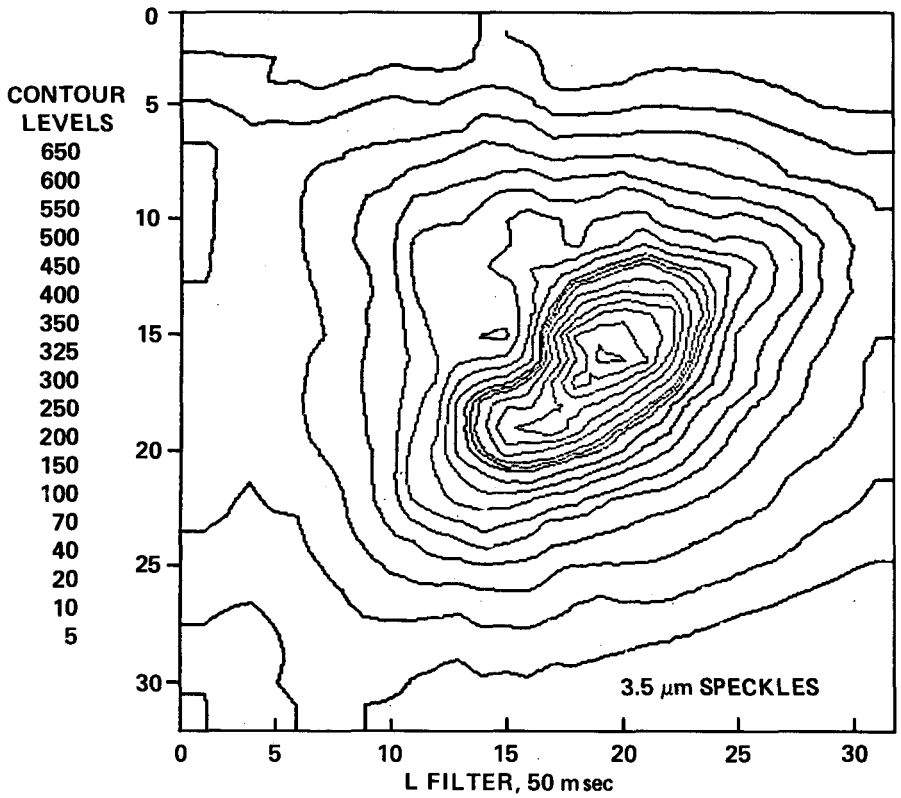

Fig. 13. 3.5 μm speckle pattern of α Ori obtained with Si:In CCD array at the IRTF. Frame time = 50 ms. Pixel numbers are indicated in the margins.

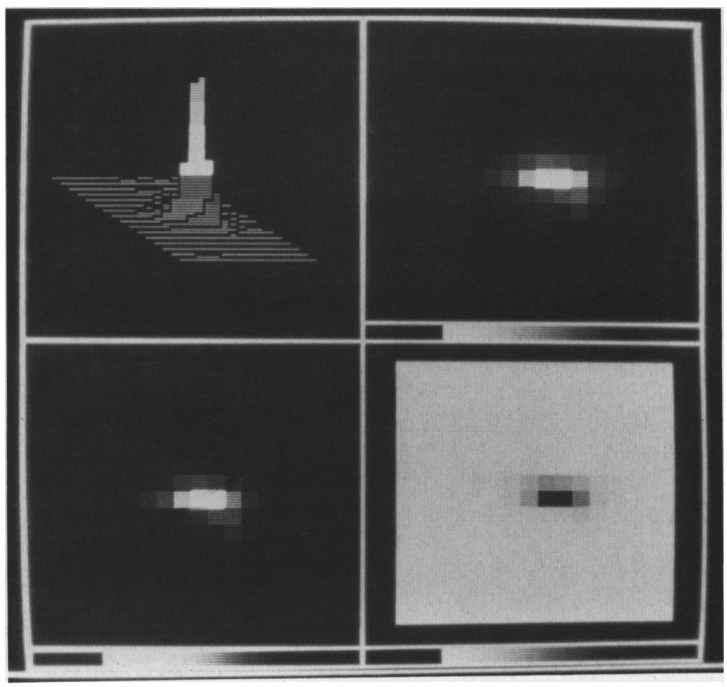

Fig. 14 3 μm Si:Bi AMCID imagery of α Ori from NASA/U. Arizona IR telescope. Clockwise from upper left, images are a histogram representation of the 16 x 16 array signal; the result of multiplying two frames; a negative (single-frame) image; and a positive (single-frame) image.

https://doi.org/10.1017/S0252921100108693 Published online by Cambridge University Press

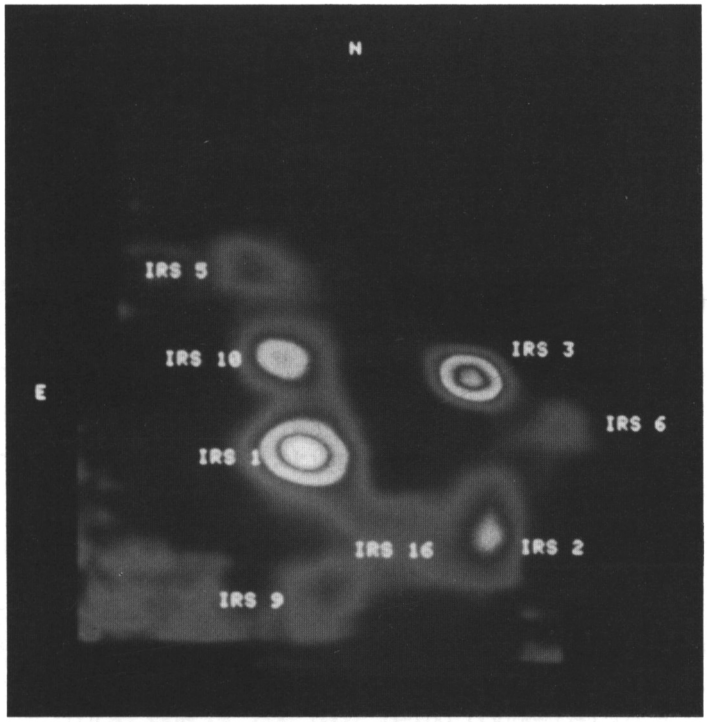

Fig. 15. 8.3 μm imagery of the Galactic Center, obtained with a 16 x 16 Si:Bi AMCID array at the IRTF. This image has not been fully processed; the elliptical shape of some of the sources (e.g. IRS1, IRS3) is a result of row-to-row crosstalk.

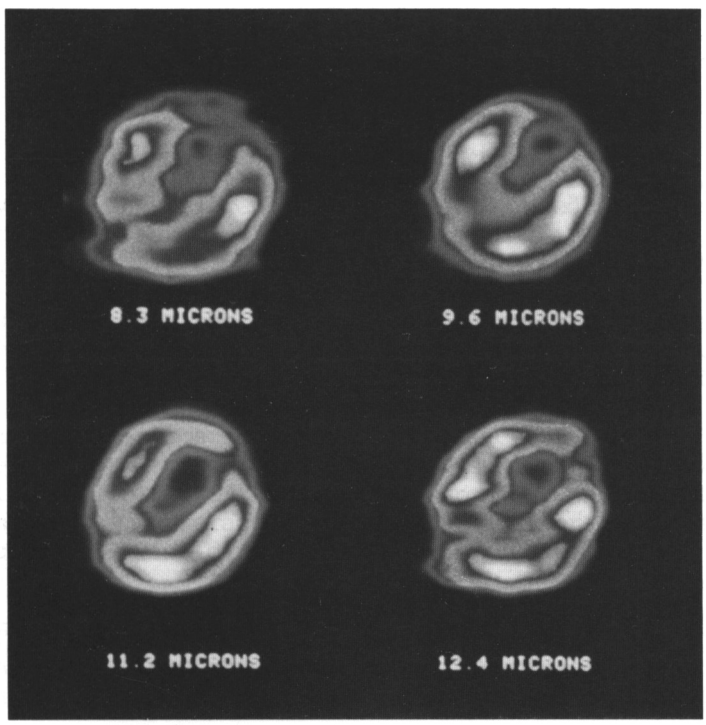

Fig. 16. IRTF AMCID imagery of NGC 7027 in four wavelength bands near 10 μm.

https://doi.org/10.1017/S0252921100108693 Published online by Cambridge University Press

DISCUSSION

A. Moorwood: How large do you think it will be possible to build CCD and CID IR arrays and what is the limiting factor?

C. McCreight: At present, 64 × 64 infrared arrays are in a state of active development. It is expected that 128 × 128 formats will be achievable in the next few years. With these arrays as "building blocks", one can in principle assemble very large IR focal planes. The factors which limit the size of arrays are associated with their large substrates: (1) achieving uniform doping and crystallinity in the detector substrate, and (2) achieving good process control (e.g. in the oxide deposition, ion implantation, and metalization steps) over large areas.

P. Léna: Could you comment on the fundmental thermodynamic limitation which will set the ultimate read-out noise?

C. McCreight: IR CCD arrays are at present a factor of two or more above fundamental sensitivity limits, which are due to fast interface state noise, detector excess noise, and output FET noise. The limiting factor for switched-FET and accumulation-mode CID arrays (kTC or reset noise, with some noise contributions from the FET) is now closely approached, for typical values of input capacitance.

https://doi.org/10.1017/S0252921100108693 Published online by Cambridge University Press